

## Numerical exploration of coherent excitation in three-level systems

H. A. Camp, M. H. Shah, M. L. Trachy, O. L. Weaver, and B. D. DePaola\*

*J. R. Macdonald Laboratory, Department of Physics, Kansas State University, Manhattan, Kansas 66506-2601, USA*

(Received 15 February 2005; published 4 May 2005)

A great deal of effort has been applied to understanding population dynamics within a variety of coherent excitation schemes. The goal in such studies has been to understand the conditions necessary for efficient transfer of population from one state to another. While many theoretical treatments include the effects of natural lifetimes that are present in any given system, some neglect this important aspect when considering specific cases. Adiabatic approximations are also widely made. Additionally, it is often difficult to envision how the different parameters controlling efficient population transfer are interrelated or even which parameters are the most critical, especially when the decay lifetimes are taken into account. This work describes a numerical study of coherent excitation applied to a  $^{87}\text{Rb}$  ladder system where spontaneous decay rates are included, and adiabaticity is not assumed. A useful method is introduced to explore the interdependence of various excitation parameters. The efficiency of population transfer as a function of several experimentally controllable parameters is explored, and other general trends are summarized.

DOI: 10.1103/PhysRevA.71.053401

PACS number(s): 32.80.Qk, 42.50.Hz

### I. INTRODUCTION

In the past two decades, significant attention has been focused on application of coherent population transfer techniques to areas ranging from quantum computing [1] to electromagnetically induced transparency [2]. A great deal of work has been done in both theory [3–5] and experiment [6–8], and a variety of coherent excitation schemes have been explored [9,10]. For the most part, the motivation behind using coherent light in such a manner has been to ensure maximum population transfer from one state to another.

While the theory of coherent population dynamics has been extensively studied, many treatments choose to neglect population lifetimes present in the system when looking at specific special cases. Additionally, many treatments that do consider population lifetimes also employ an adiabatic approximation [11]. In defense of such approaches, most experiments do not allow one to measure population dynamics during the excitation and decay of populations; hence there has been little motivation to include such loss terms when discussing efficient methods to populate a particular atomic state. However, recent experiments [12] have demonstrated the ability to measure the temporal evolution of populations during coherent excitation. Thus, there is currently an interest in theoretical models having decay terms present. A deeper understanding of the dynamics of the mechanism could yield important insights and allow better control and manipulation of coherently excited targets. Nevertheless, it is difficult to visualize and understand the relative importance and the interplay between several separate experimental parameters, even without the added complication of including spontaneous decay rates.

The goal of this paper is to discuss results from a numerical exploration of the population dynamics of a coherently excited three-level system in which spontaneous emission

rates are included and adiabaticity is not assumed. This system is closed; thus total population is preserved. The simulations do not take into account other loss mechanisms such as associative or Penning ionization [13–15] that may be present in this system, though if these rates were known, they could readily be included. It is recognized, however, that these loss mechanisms may play an important part in the accurate depiction of the population dynamics.

The numerical simulations carried out here were meant to explore experimentally accessible regions of parameter space in a ladder system of states in  $^{87}\text{Rb}$ . The primary goal of this exercise is to achieve a better understanding of how the parameters controlling efficient population transfer are interrelated. This work investigates what conditions must be present to achieve high efficiency coherent population transfer from the  $5s_{1/2}$ ,  $F=2$  ground state to the excited  $4d_{5/2}$ ,  $F=4$  state, while introducing a minimum population into the intermediate ( $5p_{3/2}$ ,  $F=3$ ) state. This work also reviews the basic theory of coherent excitation, introducing the equations of temporal evolution that govern these population transfer mechanisms, and exploring the effects of the most important experimental parameters.

### II. BASIC THEORY

One effective coherent excitation technique used in a variety of applications is known as stimulated Raman adiabatic passage (STIRAP). Other approaches, such as the application of  $\pi$  pulses [16,17], can achieve similar efficiency in population transfer; however, STIRAP is known for its robustness in terms of small variations in laser intensity, timing, and other excitation parameters. The theory of STIRAP has been studied in detail elsewhere [3,18], and therefore, only a general theoretical framework need be presented here.

The selected system of interest for this work is a three-level “ladder” excitation scheme in  $^{87}\text{Rb}$  [Fig. 1(a)]. The “pump” laser is detuned from the  $5s$ - $5p$  transition by  $\Delta_1$ , while the “Stokes” laser is detuned from the  $5p$ - $4d$  transition

---

\*Corresponding author. Email address: depaola@phys.ksu.edu

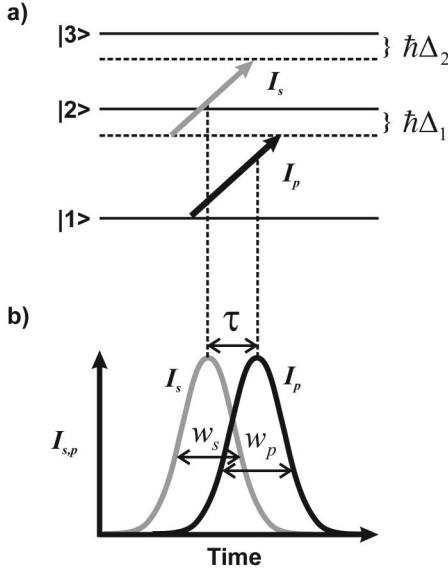


FIG. 1. A three-level ladder system for STIRAP. (a) Simplified energy level diagram. In the work of this paper,  $|1\rangle$  refers to  $5s_{1/2}F=2$ ,  $|2\rangle$  refers to  $5p_{3/2}F=3$ , and  $|3\rangle$  refers to  $4d_{5/2}F=4$  in  $^{87}\text{Rb}$ .  $\hbar\Delta_1$  and  $\hbar\Delta_2$  are the detunings from one- and two-photon resonance, respectively. (b) Counterintuitive pulse sequence for STIRAP. The “pump” pulse driving the  $5s_{1/2} \rightarrow 5p_{3/2}$  transition follows the “Stokes” pulse driving the  $5p_{3/2} \rightarrow 4d_{5/2}$  transition.

by  $\hbar\Delta_2 - \hbar\Delta_1$ , that is,  $\hbar\omega_1 + \hbar\omega_2 + \hbar\Delta_2 = E_3 - E_1$ .  $\hbar\Delta_1$  and  $\hbar\Delta_2$  are, then, the detunings from one- and two-photon resonance, respectively. The pump and Stokes lasers have Rabi frequencies of  $\Omega_p$  and  $\Omega_s$ , respectively.

### Density matrix for three-level system

Using density matrices to describe the evolution of a given system allows a phenomenological introduction of loss terms to account for spontaneous decay. In the interaction region, the Hamiltonian for the three-level system addressed in this work is given by

$$H = \frac{\hbar}{2} \begin{pmatrix} 0 & \Omega_p & 0 \\ \Omega_p & 2\Delta_1 & \Omega_s \\ 0 & \Omega_s & 2\Delta_2 \end{pmatrix}, \quad (1)$$

where the rotating-wave approximation has been used. The quantum Liouville equation, including relaxation terms to account for spontaneous emission losses, is then given [3] by

$$\hbar\dot{\rho}_{ij} = -i[H, \rho]_{ij} - \hbar[\Gamma\rho]_{ij}, \quad (2)$$

where

$$[\Gamma\rho]_{ij} = \rho_{ij} \sum_k \frac{1}{2} (A_{ik} + A_{jk}) - \delta_{ij} \sum_k \rho_{kk} A_{ki}. \quad (3)$$

Here, the  $A_{mn}$  terms are Einstein  $A$  coefficients connecting state  $m$  to  $n$ . Implied in this notation is the convention  $A_{mn} = 0$  unless  $m > n$ . Because  $\rho$  is Hermitian, and because the diagonal terms, which represent the relative population of each level, are all real, the task now consists of solving a set

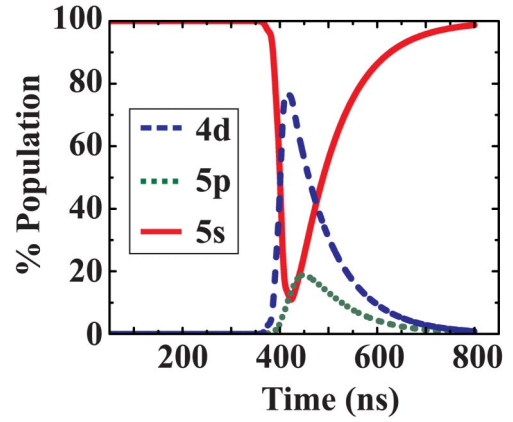


FIG. 2. Typical plot of populations versus time. Note that population in the  $5p$  level lags that in the  $4d$  level, indicative of adiabatic coherent population transfer.

of six coupled, first-order differential equations, subject to the initial conditions  $\rho_{mn} = 0$  unless  $m = n = 1$ . This was done numerically, as described below.

### III. NUMERICAL RESULTS

For the results presented here, the laser pulses were chosen to be Gaussian, although any pulse shape can be studied. The pump and Stokes lasers have pulse widths full width at half maximum of  $w_p$  and  $w_s$ , respectively. The delay between pulses,  $\tau$ , characterizes the separation in time between the centroids of the two pulses.  $\tau$  is defined to be positive when the pump pulse precedes the Stokes pulse. This is referred to as the “intuitive” pulse ordering; a negative  $\tau$  indicates a so-called “counterintuitive” pulse ordering. The pump and Stokes fields have intensities  $I_p$  and  $I_s$ , respectively. These readily measurable intensities are used as parameters in place of the related Rabi frequencies of Eq. (1). Therefore, the seven parameters of interest in this work are  $I_p, I_s, w_p, w_s, \Delta_1, \Delta_2$ , and  $\tau$ . Figures 1(a) and 1(b) illustrate the parameters of interest.

Using the MATHEMATICA software [19,20] to set up and solve the system of equations allows one to dynamically interact with the parameters of interest, selecting values and plotting the solutions in real time. Figure 2 is a typical time evolution plot, showing the populations in the  $5s, 5p$ , and  $4d$  states as a function of time for some selected values of the seven parameters of interest. Note that such a plot can yield extensive information about coherent excitation, such as whether the population transfer is in an adiabatic or diabatic regime [12]. While such plots are of great value in understanding the behavior of coherent transfer processes, they are not the focus of this work.

Using plots like that in Fig. 2, one can quickly obtain an intuitive feel for how individual parameters affect population dynamics. However, a “global” picture of multiple parameter interactions is still lacking simply because fixing all but one variable and changing only a single parameter at a time is an awkward approach to exploring this large multidimensional parameter space.

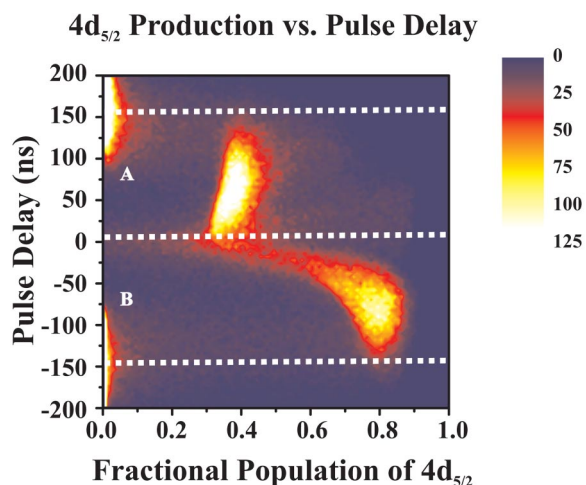


FIG. 3. Fractional  $4d_{5/2}$  production versus pulse delay. Two distinct regions exist, delineated by dotted lines, corresponding to intuitive pulse order (region A) and counterintuitive pulse order (region B).

The alternative used in this work was to randomly select values for each of the seven parameters of interest within appropriate ranges defined by typical experimental limitations. Pulse widths  $w_p$  and  $w_s$  were studied over a range from 33 to 100 ns. Pulse widths larger than 100 ns were not explored because the experimental focus [12] is on the few nanosecond time scale. Pulse widths of 33 ns are consistent with the shortest pulses typically available from acousto-optical modulators. The pulse delay  $\tau$  ranged from  $-200$  to  $200$  ns in accordance with the pulse width selection. For  $|\tau| \gg 200$ , the pump and Stokes pulses will not overlap significantly.

The pump and Stokes intensities  $I_p$  and  $I_s$  were selected to have ranges from 0 to  $100 \text{ mW/cm}^2$ , denoting a reasonable range consistent with typical cw diode laser output intensities. Similarly, one- and two-photon detunings  $\Delta_1$  and  $\Delta_2$  ranging from  $-150$  to  $150$  MHz span the detuning ranges available from acousto-optical modulators. The range for each control parameter extends sufficiently to probe the behavior of the system in depth, yet does not extend beyond what is reasonably achievable in the laboratory.

For each set of randomly selected parameters, the algorithm determines the time at which the largest fraction of population is present in the  $4d$  level. This excited-state fraction is recorded, along with the fraction of atoms in the  $5s$  and  $5p$  levels at that same time. For the data presented here, populations were calculated for 180 000 sets of parameters.

In order to develop an intuitive feeling for the interplay between the seven parameters, a particular parameter of interest was plotted versus the maximum  $4d$  population, keeping in mind that all other parameters were completely random. This is an effective integration over the remaining six parameters. In this manner, one may achieve a qualitative understanding of how a single parameter behaves with respect to maximum  $4d$  production, yet one can also see how this single parameter couples with the projection of all other parameters in general. A few such plots are included in this work, and the parameters that most strongly influence efficient coherent excitation are discussed.

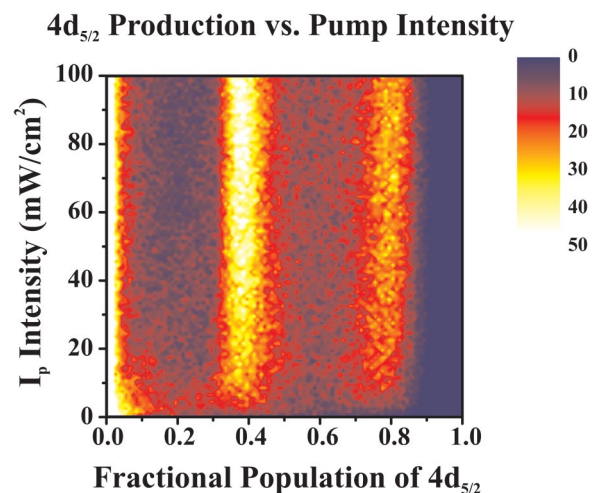


FIG. 4. Fractional  $4d_{5/2}$  production versus pump laser intensity  $I_p$ . The two visible bands at  $\sim 0.40$  and  $\sim 0.80$  correspond to the intuitive and counterintuitive pulse delay regimes, respectively.

Figure 3 shows a contour plot of  $\tau$  versus fractional  $4d$  population. The third dimension indicates how many of the 180 000 runs resulted in a particular  $4d$  fraction and a particular value of  $\tau$ . That is, the gray scale (color for online version) on this axis represents the number of data points that correspond to a given  $\tau$  and fractional  $4d$  population combination, with all other parameters taking on random values. For example, the bright area at  $\tau = 50$  ns indicates that one is most likely to obtain a fractional  $4d$  population of 0.40 throughout the random parameter space sampled by the remaining six parameters of interest. Conversely, in the dark areas it is not likely that any combination of the remaining variables will result in any population transfer into the  $4d$  state. Thus, while one does not have specific information regarding the six remaining parameters, it is clear that in order to achieve population transfer above  $\sim 0.30$  into the  $4d$  level,  $\tau$  should range between  $-150$  and  $+150$  ns. General conclusions about the other parameters of interest can be reached from these results, such as the fact that larger pulse widths cannot compensate for  $\tau$  values outside the aforementioned range.

Figure 3 also demonstrates a known idiosyncrasy of pulse order in STIRAP. Two regions, marked by dotted lines, show the intuitive delay, or pump pulse preceding the Stokes pulse, and counterintuitive delay regimes (areas labeled A and B, respectively). It is more *likely* for a given set of random parameters to yield  $4d$  population transfer in the intuitive regime, yet this intuitive configuration does not yield *efficient* population transfer, since the range of  $4d$  fraction runs from 0.25 to 0.45 for this range of  $\tau$ . On the other hand, for the counterintuitive pulse ordering, population transfer is less robust with respect to the remaining parameters, but the amount of population transferred to the  $4d$  state is *much* higher, up to 0.90. The advantage of this form of presentation is that it gives one the ability to see at a glance that pulse delay is a critical factor in determining efficient  $4d$  population transfer, and that one can not compensate for a “bad” delay by adjusting any of the other parameters.

Figure 4 is similar in construction to Fig. 3. Here, the

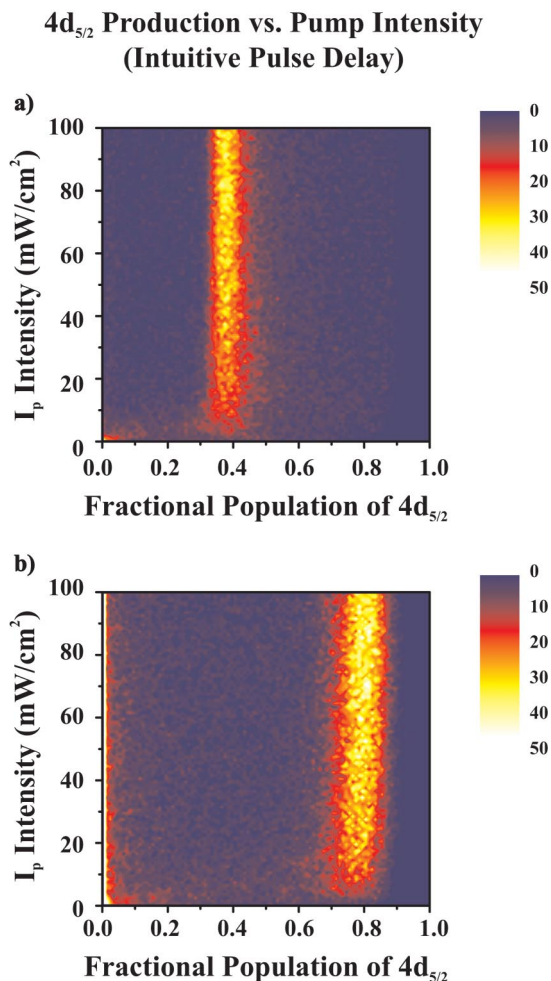


FIG. 5. Gated fractional  $4d_{5/2}$  production versus pump laser intensity  $I_p$ . (a) Only intuitive pulse order counts are plotted. (b) Only counterintuitive pulse order counts are plotted.

parameter of interest, namely, the intensity of the pump laser light,  $I_p$ , is plotted versus  $4d$  population. Two distinct regions are apparent, one showing a robust but low transfer efficiency of population ( $\sim 0.40$ ), and the other showing a less robust, but much more efficient transfer ( $\sim 0.80$ ). These bands are correlated with the state of the pulse delay. The band at 0.40 results from the intuitive pulse delay configuration, while the band at 0.80 corresponds to the counterintuitive configuration. This conclusion can be verified by selectively plotting data for which  $\tau$  takes on values in the intuitive or counterintuitive regime, as shown in Fig. 5. In practice, this was done by taking “cuts” in the seven-dimensional parameter space for which  $\tau$  lies in either region A or B of Fig. 3. The intuitive pulse order is plotted in Fig. 5(a), where pulse delay was limited to a range from 25 to 150 ns. Figure 5(b) shows results when the pulse delay ranged from  $-150$  to  $-50$  ns. Again, it is evident how critical  $\tau$  can be as it gives rise to two distinct parameter regions in each of the other six variable plots.

Close inspection of Fig. 4 or 5 indicates that for  $I_p > 20$  W/cm<sup>2</sup>,  $I_p$  does not seem to be a critical parameter for efficient production of  $4d$ . Intensities below  $\sim 5$  mW/cm<sup>2</sup> result in much less robust, but not much less efficient,  $4d$

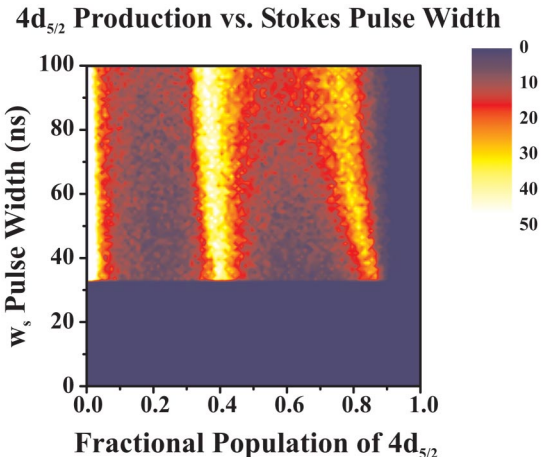


FIG. 6. Fractional  $4d_{5/2}$  production as a function of Stokes pulse width.

production. Plotting the intensity of the Stokes laser light,  $I_s$ , yields similar results to Figs. 4 and 5.

Figure 6 shows the Stokes laser pulse width  $w_s$  versus fractional  $4d$  population. As  $w_s$  decreases, population is transferred to the  $4d$  level more efficiently in both the intuiti-

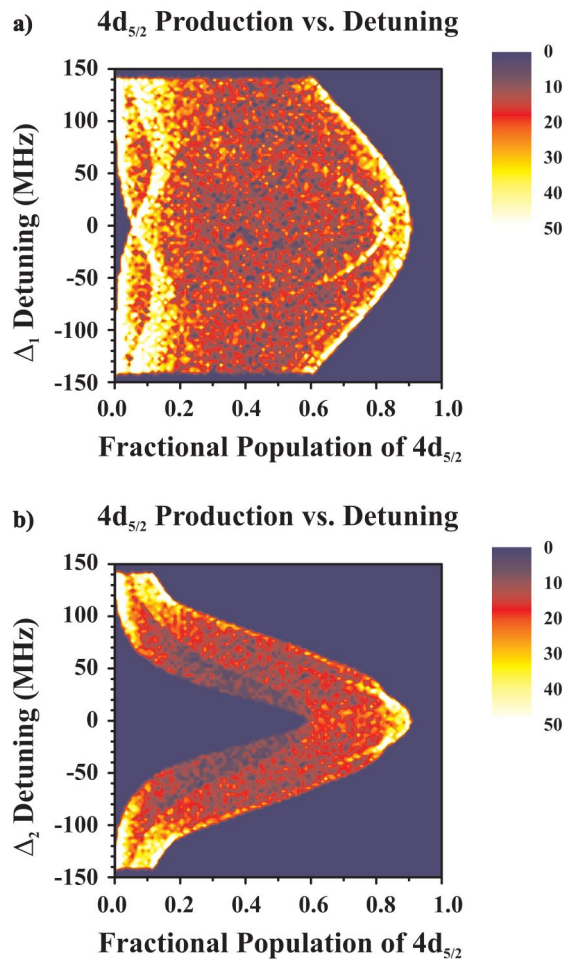


FIG. 7. Fractional  $4d_{5/2}$  production as a function of detuning. (a) Single-photon detuning  $\Delta_1$ . (b) Two-photon detuning  $\Delta_2$ . Parameters for these two specific cases are listed in the text.

tive and counterintuitive regimes. Also, both regime bands narrow as pulse width decreases, indicating that the acceptable range of the other six parameters is decreasing. The counterintuitive pulse regime appears to be affected by the Stokes pulse width more than the intuitive pulse regime, as indicated in the sharpness of curvature evident in the band at  $\sim 0.80$ .

Because no adiabatic approximation has been made, one could explore adiabatic or diabatic transfer regimes by selecting combinations of laser pulse widths and intensities. In general, the more narrow  $w_p$  and  $w_s$  become, the more diabatic the process becomes. Similarly, diabaticity increases as intensities  $I_p$  and  $I_s$  increase, for fixed pulse widths. Exploration of adiabatic versus diabatic behavior can thus be achieved by selecting combinations of laser intensity and pulse width to study particular regions of interest.

In order to accentuate the relative importance of one- and two-photon detuning, data can be plotted for fixed selected delay, pump and Stokes pulse widths, and intensities [21], while varying both  $\Delta_1$  and  $\Delta_2$ . The results shown in Figs. 7(a) and 7(b) indicate that single-photon detuning is much less important than two-photon detuning, a result consistent with previous calculations [18]. In a series of plots showing  $\Delta_1$  and  $\Delta_2$  versus fractional  $4d$  population for different values of  $I_p$  and  $I_s$ , the curvature of the bands was seen to

greatly increase as the intensities decreased. That is, for efficient population transfer, larger values of laser intensity require smaller values of one- and two-photon detunings.

#### IV. SUMMARY

This work has shown the behavior of coherent population dynamics when population lifetimes are taken into account, and examines the interdependence of various critical parameters in achieving efficient population transfer to the target excited state. The techniques presented here allow one to explore population transfer behavior as a function of a variety of separate parameters, and, through the use of indicious projections of the data, analyze the inherent interdependencies of this seven-dimensional space. It is evident from the data presented here that pulse timing is the most critical parameter in efficient population transfer, while other variables, such as laser intensities, are much less restrictive.

#### ACKNOWLEDGMENTS

This work was supported by the Chemical Sciences, Geosciences and Biosciences Division, Office of Basic Energy Sciences, Office of Science, U.S. Department of Energy.

- 
- [1] M. D. Lukin *et al.*, Phys. Rev. Lett. **87**, 037901 (2001).
  - [2] M. D. Stenner, D. J. Gauthier, and M. A. Neifeld, Nature (London) **425**, 695 (2003).
  - [3] B. W. Shore, *The Theory of Coherent Atomic Excitation* (John Wiley and Sons, New York, 1990), vol. 2.
  - [4] R. G. Brewer and E. L. Hahn, Phys. Rev. A **11**, 1641 (1975).
  - [5] R. N. Shakhmuratov and J. Odeurs, Phys. Rev. A **68**, 043802 (2003).
  - [6] B. Broers, H. B. van Linden vanden Heuvel, and L. D. Noordam, Phys. Rev. Lett. **69**, 2062 (1992).
  - [7] W. Süptitz, B. C. Duncan, and P. L. Gould, J. Opt. Soc. Am. B **14**, 1001 (1997).
  - [8] F. Vewinger, M. Heinz, R. Garcia Fernandez, N. V. Vitanov, and K. Bergmann, Phys. Rev. Lett. **91**, 213001 (2003).
  - [9] R. G. Unanyan, M. E. Pietrzyk, B. W. Shore, and K. Bergmann, Phys. Rev. A **70**, 053404 (2004).
  - [10] L. P. Yatsenko, S. Guérin, and H. R. Jauslin, Phys. Rev. A **65**, 043407 (2002).
  - [11] Y. B. Band, Phys. Rev. A **45**, 6643 (1992).
  - [12] H. A. Camp *et al.* (unpublished).
  - [13] M. Chéret, L. Barbier, W. Lindinger, and R. Deloche, J. Phys. B **15**, 3463 (1982).
  - [14] L. Barbier and M. Chéret, J. Phys. B **20**, 1229 (1987).
  - [15] P. D. Lett, P. S. Jessen, W. D. Phillips, S. L. Rolston, C. I. Westbrook, and P. L. Gould, Phys. Rev. Lett. **67**, 2139 (1991).
  - [16] D. Felinto, L. H. Acioli, and S. S. Vianna, Phys. Rev. A **70**, 043403 (2004).
  - [17] I. Roos and K. Molmer, Phys. Rev. A **69**, 022321 (2004).
  - [18] N. V. Vitanov, T. Halfmann, B. W. Shore, and K. Bergmann, Annu. Rev. Phys. Chem. **52**, 763 (2001).
  - [19] Wolfram Research, Inc., computer code MATHEMATICA, version 5.1, Champaign, IL, 2004.
  - [20] This simple MATHEMATICA code is available upon request.
  - [21] For Fig. 7, the pulse delay was fixed at  $-80$  ns, and both pulse widths  $w_1$  and  $w_2$  were fixed at 50 ns. The pump intensity  $I_p$  was set to be  $20$  W/cm<sup>2</sup>, and the Stokes intensity  $I_2$  was set so that the Rabi frequencies  $\Omega_s$  and  $\Omega_p$  are equal. Both  $\Delta_1$  and  $\Delta_2$  (one- and two-photon resonance, respectively) were allowed to vary.